EXPERIMENTAL DETERMINATION OF TEMPERATURE IN SHOCK-COMPRESSED NaCl AND KCl AND OF THEIR MELTING CURVES AT PRESSURES UP TO 700 kbar

S. B. KORMER, M. V. SINITSYN, G. A. KIRILLOV, and V. D. URLIN

Submitted to JETP editor November 5, 1964

J. Exptl. Theoret. Phys. (U.S.S.R.) 48, 1033-1049 (April, 1965)

The temperature of shock-compressed ionic crystals of NaCl and KCl was measured in the solid and liquid phase regions at pressures up to 800 kbar. The maximum measured temperatures amounted to 5500° K. The melting curves of NaCl at pressures from 540 to 700 kbar and of KCl from 330 to 480 kbar were determined experimentally. The melting point at these pressures rose to about 4000° K, i.e., by a factor of 4. It was estimated that the entropy change when melting under these conditions was close to that found at atmospheric pressure, but the volume change amounted to 2—4% instead of 20%. It was shown experimentally that melting does not produce the two-wave configuration in the investigated substances.

INTRODUCTION

DYNAMIC methods of investigating the properties of condensed matter at high pressures and temperatures are currently being successfully developed. By measuring the kinematic parameters of a shock wave—its velocity D and the mass velocity of matter behind the front u—we can find, from the well-known laws of conservation, the pressure P, the density ρ and the increase in the internal energy E.[1,2] The temperature T is then determined by calculation using some particular equation of state of matter.[1,3-7] The direct measurement of the temperature of condensed substances under shock-compression conditions makes it possible to extend and refine our knowledge of the equation of state.

At temperatures of the order of several thousands or even tens of thousands of degrees, reached under shock compression, the optical methods of measurement are best. Therefore, there is special interest in the class of transparent substances, in which it is possible to record the light emission of a shock-wave front during its propagation through a layer of still uncompressed matter.[8] Examples of such substances, investigated in the present study, are single crystals of NaCl and KCl, whose dynamic adiabats in the range of pressures considered here have been reported earlier in [4,6] At present, temperatures in shock-compressed metals measured only during their expansion, because metals are opaque.[9,10]

The brightness temperatures of the shock-wave front were determined at two wavelengths (4780 and 6250 Å) by comparison of the light fluxes emitted by the front and by a standard source of light, using a specially developed photoelectric apparatus. To obtain the true temperatures from the measured brightness temperatures, it is necessary to know the emissivity of the shock-wave front a. It may differ from unity both due to the transparency τ of the substance behind the shock-wave front, and due to its reflectivity r ($a = 1 - \tau - r$). Experiments showed that the investigated ionic crystals became opaque in layers whose thicknesses are considerably less than those at which layers of shock-compressed gases became opaque.[11] This makes it possible either to neglect the transparency, beginning from some thickness of the compressed substance, or to make the necessary correction, which does not exceed 10% of the measured temperature. In the range of pressures up to 1 Mbar, the reflectivity of a shock wave, determined experimentally in the same way as in [12], was found to be low and estimates showed that it could be neglected in the determination of the true temperature.

The most important result of the present study was the determination of the melting curves of NaCl and KCl at pressures of about 500—700 kbar. Obviously, when the shock-wave pressure increases the temperature in the front rises and, beginning from certain pressures, the initially solid substance melts. Up to now the melting in the shock-wave front has not been allowed for in describing the state of shock-compressed substances. This is understandable because the melting affects little the kinematic parameters of the shock-wave front or the position of the

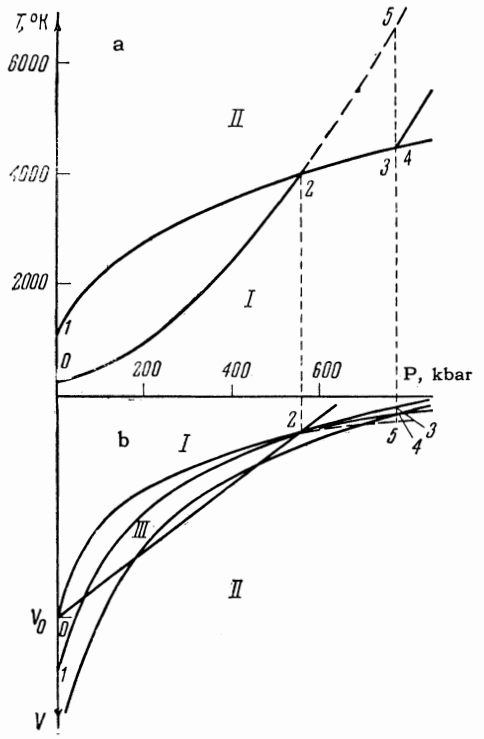

FIG. 1. Shock adiabat of a substance in a two-phase region (solid–liquid). I) Solid phase, II) liquid phase, III) region of coexistence of the two phases. The dashed curve represents the shock adiabat of the "superheated" solid phase.

dynamic adiabat in the P–V coordinates.[13] On the other hand, temperature was found to be much more sensitive to melting.

Figure 1a shows, by way of example, the phase diagram of NaCl. The melting curve 1–2–4, found from Simon's equation

$$P = P_0 + A[(T/T_0)^q - 1] \qquad (1)$$

(where $T_0 = 1073°$ K is the melting point at atmospheric pressure, $P_0 = 0$, $A = 16.7$ kbar, and $q = 2.7$ are Simon's coefficients[14]) separates the solid from the liquid state. The dynamic adiabat 0–2–5 is plotted from the data given in [7] on the assumption that there is no melting. Beginning from some pressure P_2, the thermal energy is sufficient for the melting of NaCl to begin. The further course of the dependence T(P) along the dynamic adiabat may be explained by analogy with the melting under constant pressure, when, after the beginning of melting, the energy supplied does not raise the temperature until the melting process ends. Further heating again produces a temperature rise. Similar behavior should be observed under shock compression. Here, an increase in the wave-front pressure is accompanied by an increase in the thermal energy. Some rise of temperature in the section 2–4 in Fig. 1a is to be expected as a result of the increase in the pressure.

We shall estimate the possible difference between temperatures at points 5 (shock adiabat without allowance for melting) and 3, 4 (with allowance for melting). From the conditions of equilibrium between two phases of a substance (equality of temperatures, pressures, and chemical potentials), we can write

$$H_4 = H_3 - T_3\Delta S \qquad (2)$$

or

$$E_4 = E_3 + T_3\Delta S - P_3\Delta V. \qquad (3)$$

Here, the subscript "3" represents the solid phase and "4" the liquid phase along the melting curve, H is the enthalpy, E is the total internal energy, $T_3\Delta S = L$ is the latent heat of fusion, $\Delta S = S_4 - S_3$ is the change in the entropy on melting, $\Delta V = V_4 - V_3$ is the sudden change in the specific volume on melting. Since $E = E_C + E_T$, where E_C is the elastic compression energy, and E_T is the energy used to heat the substance, we can rewrite Eq. (3) in the form

$$E_{T4} - E_{T3} = T_3\Delta S - (P_3 - \bar{P}_c)\Delta V,$$
$$\bar{P}_c = [E_x(V_3) - E_x(V_4)]/\Delta V. \qquad (4)$$

Neglecting the small difference, in the P–V coordinates, between the dynamic adiabat of the "superheated" solid phase and the adiabat in the region of coexistence of phases (cf. Fig. 1b), we can write $E_{T5} = E_{T4}$. Using this relationship and dividing the left-hand and right-hand parts of Eq. (4) by the specific heat $C_V = 3Rn$ (where n is the number of atoms in a molecule), we obtain

$$T_5 - T_3 = T_3\left[\frac{\Delta S}{3Rn} - \frac{(P_3 - \bar{P}_c)V_3}{3RnT_3\gamma}\gamma\frac{\Delta V}{V_3}\right]. \qquad (5)$$

The second term in square brackets does not exceed 10% of the first term:

$$\frac{(P_3 - \bar{P}_c)V_3}{3RnT_3\gamma} \approx 1, \quad \frac{\Delta V}{V_3} \sim 0.03, \quad \gamma \sim 1.5, \quad \frac{\Delta S}{3Rn} \approx 0.5.$$

Hence

$$T_5 - T_3 \approx T_3\Delta S/3Rn = L/3Rn. \qquad (6)$$

It follows from Eq. (6) that the allowance for melting leads to a fall in the temperature in the liquid phase, compared with the values calculated without such an allowance, by an amount equal to the latent heat of fusion divided by the specific heat. For the majority of simple substances and inorganic compounds, the sudden change in the entropy on melting varies, under normal conditions, within a fairly narrow range and amounts to $\frac{1}{3}$ – $\frac{1}{2}$ of the specific heat of the substance. We

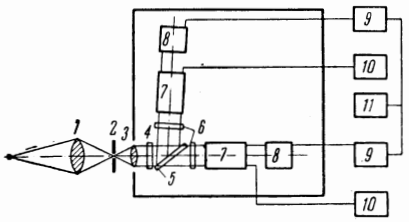

FIG. 2. Block diagram of the apparatus: 1), 3) objectives, 2) diaphragm, 4) neutral light filters, 5) beam splitters, 6) selective light filters, 7) photomultipliers, 8) cathode followers, 9) OK-17 oscillographs, 10) VS-9 rectifiers, 11) GSS-6 oscillator.

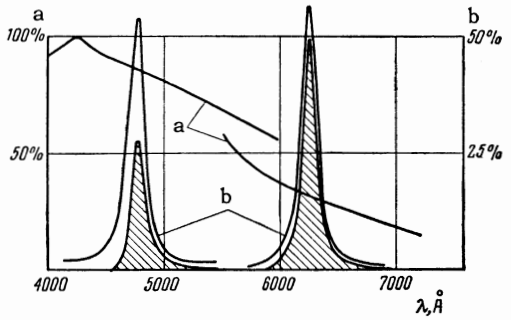

FIG. 3. Spectral characteristics of the photomultipliers (a) and of selective light filters (b).

shall use this and assume that when a substance is compressed, the sudden change in its entropy remains constant irrespective of the applied pressure. Such an assumption is analogous to that made by Gilbarry,[15] who extended Lindemann's rule[16] to the properties of substances at high pressures. Assuming for NaCl the values $\Delta S/3Rn = 0.5$ and $T_3 = 4450$ (cf. Fig. 1a), we find that $T_5 - T_3 = 2200°$ K.

It follows from this estimate that temperature is very sensitive to the process of melting. A similar conclusion has been reached by Urlin[17] from an analysis of the melting of metals in a shock-wave front, using the equations of state for the solid and liquid phases of a substance. The error of this method of temperature measurement ($\approx 200°$ K) is much less than the expected effect and this makes it possible to establish clearly the latter's presence.

METHOD OF MEASUREMENT

The temperature behind the shock-wave front during the propagation of a shock wave through a substance was determined by an optical method,[18] which was based on a comparison of the light fluxes emitted by the compressed substance and by a standard source of light. In the apparatus developed by the present authors, the light emission is recorded in two parts of the spectrum. The block diagram of the apparatus is given in Fig. 2.

The first objective 1 (Telemar-2 type, with a focal length $F_1 = 750$ mm and a relative aperture $C_1 = 1:6.3$) projected the image of a source of light on to a diaphragm 2, which cut out extraneous light. The diaphragm was placed at the focus of a second objective 3 (Tessar type, with $F_2 = 210$ mm and $C_2 = 1:6.3$), which ensured that the beam was practically parallel behind this objective. Photomultipliers (PM) were placed at such a distance from the optical system that the image of the entrance lens of the first objective was projected on to their photocathodes. The constant distance between the apparatus and the test sample ensured the constancy of the dimensions of the image formed by the entrance lens of the first objective on the photocathode and the uniformity of the image illumination. This avoided the influence of the band characteristic of the photocathode sensitivity on the results obtained. A plate of colorless optical glass 5, placed at an angle of 60° to the light beam, split it approximately into two equal halves which went to the two PM's (7). The use of PM's makes it possible to lower considerably the threshold of measurable temperatures, compared with the photographic method.[11] The use of explosive changes, which made it necessary to place the measuring instruments relatively far (10 m) from the test sample, and the use of light filters with a narrow pass band (100 Å), raised the lower limit of the measurable temperatures to 1500—2000° K. Then the PM received a light flux of 5×10^{-2} erg/sec. This high sensitivity of the apparatus was achieved by the use of PM's with a high quantum yield of the photocathode,[19] developed at the present authors' request.

The signal from the PM's was recorded by an oscillograph 9 (type OK-17), which was able to handle a pulse with a rise time of 5×10^{-8} sec.

To select a narrow range of wavelengths in the blue and red part of the visible spectrum, we used interference light filters, whose transmission maxima corresponded, respectively, to 4780 and 6250 Å. The transmission curves of the filters, determined with an SF-4 spectrophotometer, are shown in Fig. 3. To improve the spectral characteristics, the interference light filters were combined with glass filters. The overall transmission is shown hatched in Fig. 3. The same figure includes the spectral sensitivity characteristic of the PM's used in the present work, as reported in [19]. The intensity of the light flux incident on a PM was controlled, if necessary, by neutral light filters, whose transmission spectra were also determined with a SF-4.

Table I

λ, Å	T, ° K		
	2500	4000	7000
4780	2	3	5.5
6250	2.5	3.5	6

The standard source of light was a ribbon-filament lamp of the SI-16 type, calibrated at VNIIM (D. I. Mendeleev All-Union Metrology Research Institute) and systematically checked with an optical pyrometer (type OP-48). An IFK-50 pulse-discharge lamp was used as the intermediate standard (cf. [20]). It was necessary to use this lamp because the ribbon-filament lamp temperature was low and its luminous area small. The brightness temperature of the IFK-50 lamp, measured with the same apparatus, was found to be 6900° K at λ = 4780 Å and 6200° K at λ = 6250 Å.

In the temperature measurements, the conditions were selected so as to ensure that the photomultipliers were working in the linear part of their optical characteristic, and the oscillograph was used in the linear part of its amplitude characteristic. Then the signal amplitude on the oscillograph screen was

$$h = \alpha K s A, \tag{7}$$

where α is a constant representing the amplification factor of the system, s is the area of the luminous object, and K is the transmission coefficient of the neutral filters.

The actinic flux A, introduced in [21] for convenience in analysis of the experimental data, is related to temperature by

$$A = \int_{\lambda_1}^{\lambda_2} \tau(\lambda) b(\lambda) c_1 \lambda^{-5} (e^{c_2/\lambda T} - 1)^{-1} d\lambda, \tag{8}$$

where c_1 and c_2 are the radiation constants; λ_1 and λ_2 are the limits of transmission of the selective light filter; $\tau(\lambda)$ is the spectral transmission of the light filters; $b(\lambda)$ is the spectral sensitivity of the photocathode. For a known actinic flux from the standard lamp IFK-50 and for a constant coefficient α (which was true in our experiments), the actinic flux, corresponding to the measured temperature of a shock-compressed crystal, was given by the relationship

$$A_{cr} = \frac{h_{cr} s_{IFK} K_{IFK}}{h_{IFK} K_{cr} s_{cr}} A_{IFK}. \tag{9}$$

From the actinic flux obtained in this way, the required brightness temperature was found using Eq. (8). The accuracy of the method was estimated from Eqs. (8) and (9), bearing in mind that the standard temperature of the IFK-50 lamp was determined to within 5%, and the signal and amplitude h, the transmission coefficient of the neutral filters K and the area of the luminous object s could be measured to within 2%. The errors (in %) for the range of temperatures and wavelengths of interest to us are listed in Table I.

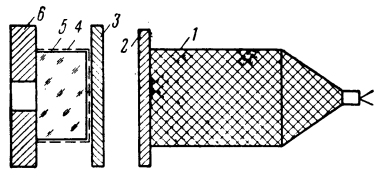

FIG. 4. Diagram showing the arrangement for temperature measurement (explanations are given in text).

TEST ARRANGEMENTS AND EXPERIMENTAL RESULTS

The NaCl and KCl samples used in the temperature measurements were single crystals [1)], measuring 40 × 40 × 20 mm and having faces of 40 × 40 mm, polished and coated with transparent Zapon lacquer to protect them from moisture. The transmission of light by the crystals was not less than 95%. Shock waves were generated in the crystals by the impact of a metal plate accelerated, by detonating an explosive, to a velocity W. A typical test arrangement is shown in Fig. 4.

The intensity of the shock wave produced in a crystal 5 was varied by varying the explosive power (1 in Fig. 4), and the materials and thicknesses of the striker 2 and the screen 3. Since the majority of the temperature measurements was carried out using explosion-driven devices developed earlier, [3,22] the shock-wave parameters were determined only if the test conditions differed from those described in [4,6] by a change in the screen material or the composition of the explosive. Then the shock-wave pressure was determined by measuring the wave velocity and using the data given in [4,6]. In two cases, we also measured the velocity of the striker plate. In one series of tests on a KCl crystal, the explosive charge was in contact with an aluminum screen. The materials and thicknesses of the screen and the striker, and the striker velocities are listed in Table II.

The screen plate 3 was used to vary the pres-

[1)]Single crystals were grown and polished at GOMZ (State Optico-Mechanical Works).

Table II

Parameters of striker plate*			Parameters of screen*		Parameters of investigated substance						
					D,	P,	ρ/ρ_0	$T_{brightness}$, °K		T, °K	
M	mm	W, km/sec	M	l, mm	km/sec	kbar		λ=4780 Å	λ=6250 Å	λ=4780 Å	λ=6250 Å
NaCl, ρ_0=2.165 g/cm³											
Al	4	5.02	Al	0.2	7.40	465	1.65	2400	2250	2650	2450
Al	4	5.40	Al	0.2	7.59	500	1.67	2950	2750	3000	2850
Al	2	5.64	Al	0.2	7.85	547	1.70	3450	3200	3500	3350
Al	2	6.06	Al	0.2	8.13	615	1.75	3450	3250	3550	3400
Fe	1.5	5.20	Fe	1.5	8.52	705	1.81	3850	3600	4000	3800
Fe	1.5	5.60	Fe	1.5	8.91	790	1.85	4800	4400	5000	4700
KCl, ρ_0=1.994 g/cm³											
Al	—	3.34**	Al	23.5	5.64	237	1.60	2350	2150	2350	2150
Al	4	5.40	W	1.8	5.75	250	1.62	2500	2300	2500	2300
Al	4	5.02	Cu	2.5	6.10	290	1.65	3500	3200	3500	3200
Al	4	5.40	Cu	2.5	6.53	353	1.71	3900	3750	3900	3750
Al	4	5.02	Al	0.2	7.00	427	1.78	3900	3700	3900	3700
Al	4	5.40	Al	0.2	7.36	485	1.81	4250	3900	4250	3900
Al	2	5.64	Al	0.2	7.50	508	1.83	4650	4250	4800	4450
Al	2	6.06	Al	0.2	7.77	560	1.86	5600	5300	5650	5350

*Here M denotes material, l – thickness, and v – velocity.
**Mass velocity in screen, doubled

sure and to screen the crystal from the light excited by the shock wave in air, and propagated in front of the striker plate 2. A layer of black paint 4, 0.1 mm thick, was used to protect the crystal from extraneous light and to eliminate the air gap between the crystal and the screen. The dimensions of the crystals ensured that the shock-wave front is as free from side loads[23] over a base of 15—12 mm, within the limits of the aperture in the diaphragm 6 (10—15 mm diameter), which was quite sufficient since the maximum value of the brightness of the front was reached much earlier. The uniformity of the light emission from the shock-wave front, within the limits of the diaphragm aperture, was checked for all types of explosive charge by photographing the aperture in white light using a photorecorder of the SFR-2 type. In all cases, the light emission was practically uniform: the blackening of the photographic film at various parts of the wave front at any given moment did not differ by more than 0.05. Estimates showed that the nonuniformity of the brightness leading to a change in the blackening by 0.2 over 10% of the area of the shock-wave front would not alter the average brightness temperature by more than 1% over the whole range of investigated temperatures.

Typical oscillograms obtained during the temperature measurements in NaCl and KCl at various shock-wave intensities, using various explosion-driven devices, are given in Fig. 5. The oscillograms show that four periods can be easily distinguished in the recorded light emission (cf. the schematic representation of the oscillogram and the x—t diagram in Fig. 6, where x is the distance and t is time). During the first period, the radiation brightness rises due to an increase in the thickness of the layer compressed by the shock wave. The duration of this period is governed primarily by the transparency of the com-

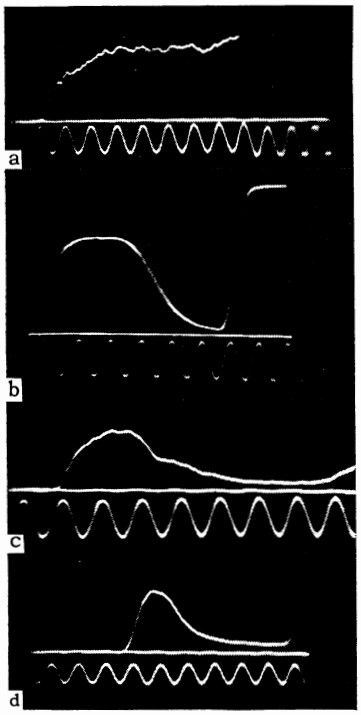

FIG. 5. Oscillograms of the light emission by the shock-wave front in KCl: a) explosive charge in contact with the screen, b) striker thickness 4 mm, c) striker thickness 2 mm; and in NaCl: d) striker thickness 2 mm. The direction of scanning is from left to right. Frequency of time marks: 2 Mc.

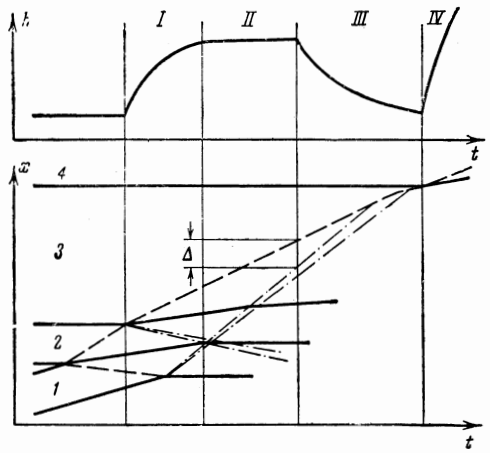

FIG. 6. Dependence of the brightness of the light emission on time and its relationship with the wave propagation in a crystal: 1) striker; 2) screen; 3) crystal; 4) air. The continuous lines show boundaries, the dashed lines show shock waves, and the chain lines show rarefaction waves.

pressed substance. The duration of the constant brightness period (II) is governed both by the transparency of the compressed substance and by the time at which a rarefaction wave enters the crystal. When the distance between the shock-wave front and the rarefaction wave overtaking it becomes approximately equal to the thickness of an opaque layer in the compressed substance Δ, the radiation intensity decreases (period III) [2)] until the shock wave, emerging at a free surface of the crystal, generates a shock wave in air with a high temperature in its front (period IV). The constancy of the brightness (Fig. 5a, b, c) means that the layer of substance behind the wave front has become practically opaque [3)] and the measured brightness temperature under these conditions is equal to the true equilibrium temperature of the compressed substance.

In fact in this case the two temperatures may differ only because of the reflection of light from the front of the wave. The reflection coefficient measured in KCl at a pressure of 425 kbar by the method proposed in [12] was found to be 1.5%, and even smaller for NaCl. The estimates obtained showed that even in the strongest shock waves used in the present study the reflection coefficient of the wave front did not exceed 2—3%, so that at all temperatures up to 5500° K the correction to the measured temperature was less than 1%. Therefore, no correction was made for reflection.

The absence of a constant-brightness period (Fig. 5d) indicates that the wave from the screen enters the crystal before the substance behind the shock-wave front becomes opaque (low absorption coefficient or slight thickness of the compressed layer). In this case, the absorption coefficient of the substance behind the shock-wave front was calculated from the rise in the radiation brightness, using the method described in [11], and the emissivity was calculated at the moment of entrance of the rarefaction wave into the crystal. The true temperature was calculated from the

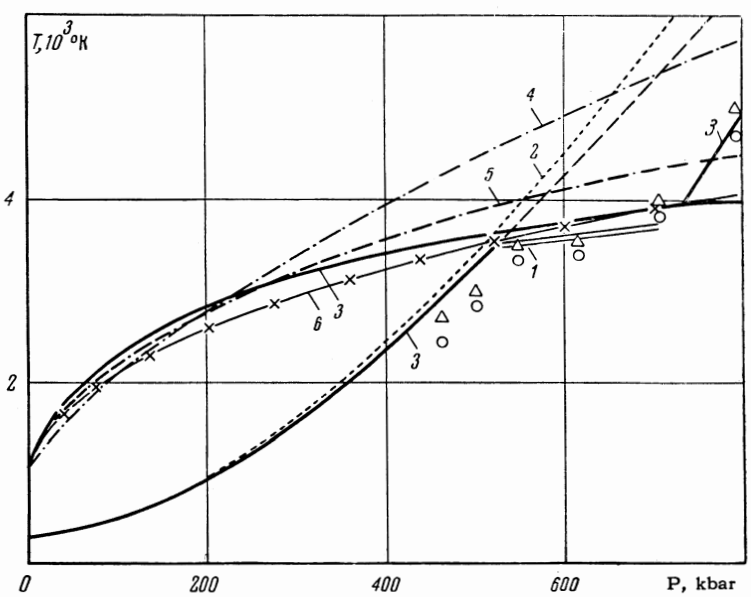

FIG. 7. Results of temperature measurement in NaCl: Δ – at λ = 4780 Å, o – at 6250 Å, 1) experimental part of the melting curve, 2) calculated data from[7], 3) calculations in present study, 4) calculations in accordance with Lindemann, 5) extrapolation of data from[14], 6) calculation using Simon's equation and parameters found in the present study.

[2)] When the substance behind a shock-wave front has a high absorption coefficient, the fall-off in the emission may be used for measuring the velocity of propagation of acoustic perturbations by the method of pressure release by an overtaking wave[23].

[3)] The present authors are proposing to deal with the phenomenon of a large reduction in the transparency of a substance behind a shock-wave front in a communication to be published in the near future.

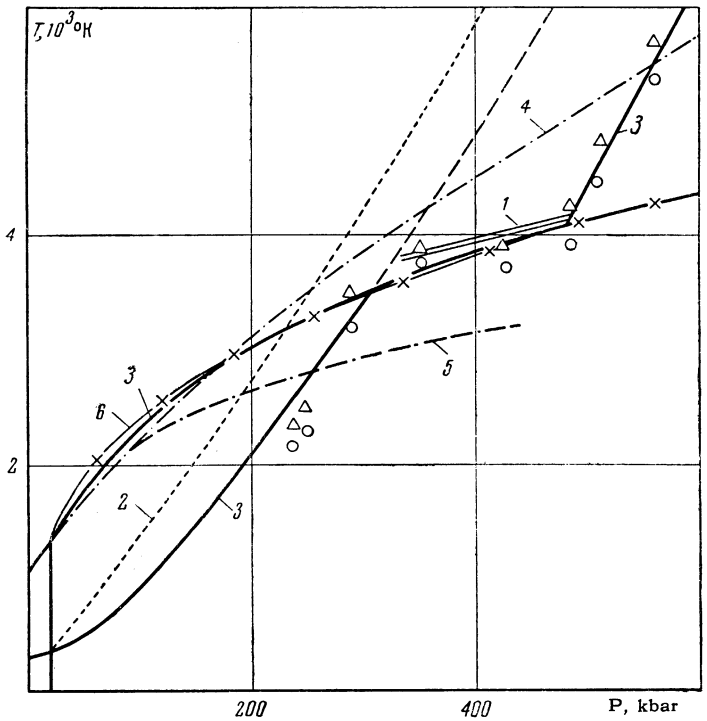

FIG. 8. Results of temperature measurement in KCl; the notation is the same as in Fig. 7, except that curve 2 is plotted using the data from[6].

brightness temperature and emissivity at the moment of maximum brightness. Allowance for the emissivity was essential in the determination of the true temperature of NaCl (Fig. 5d) in all the series of tests. For KCl, this allowance was necessary only at two points at the highest pressures, when the shock wave, as in the majority of tests on NaCl, was produced by a thin striker plate.

The results of the temperature measurements in NaCl and KCl are listed in Table II and in Figs. 7 and 8. Table II gives the average values (of four-five measurements) of the brightness and true temperatures. The difference between these temperatures is determined by the correction for the deviation of the emissivity from unity.

It should be mentioned that in all cases the temperatures measured in the blue part of the spectrum were higher than in the red part. This is not due to the fact that the shock-wave front does not behave as a black body (see above). The difference between temperatures obviously represents the accuracy of measurements.

DISCUSSION OF RESULTS

The phase diagrams of NaCl and KCl are given in Figs. 7 and 8. The experimental results obtained show clearly that both crystals melt behind the shock-wave front (cf. Introduction). NaCl begins to melt at P ≈ 540 kbar and T ≈ 3500° K, and becomes completely liquid at P ≈ 700 kbar and T ≈ 3700° K. In KCl, the beginning and end of the melting correspond, respectively, to P ≈ 330 kbar, T ≈ 3800° K and P ≈ 480 kbar, T ≈ 4100° K. [4)] The same figures include, for comparison, the calculated dynamic adiabats taken from [7] for NaCl and from [6] for KCl. The greatest difference between the experimental and calculated temperatures (up to 2000—3000 deg K) is observed at the points of complete melting. This difference is due to the lack of allowance for melting in a shock-compressed substance in the two cited papers.

Let us analyze first the experimental data which represent the behavior of NaCl and KCl in the solid phase. Considering the region of temperatures below 10^4° K, we shall write the free energy of a solid ionic crystal in the form [4,7]

$$F_I = E_c(\rho) + 6RT \ln \frac{\Theta(\rho)}{T}, \qquad (10)$$

where R is the gas constant and the Debye temperature is

$$\Theta \sim \delta^{1/2}\left(\frac{dP_c}{d\rho} - \frac{2P_c}{3\rho}\right)^{1/2}, \qquad P_c = \rho^2 \frac{dE_c}{d\rho} = \sum a_i \delta^{i/3+1}$$

($\delta = \rho/\rho_c$, where ρ_c is the density of the crystal

[4)] The results obtained indicate that the anomalies, reported in[7], in the dynamic adiabats of NaCl and KCl occur when these substances are known to be in the liquid phase.

Table III

	NaCl	KCl I	KCl II
ρ_C, g/cm^3	2.218	2.046	2.36
a_1, Mbar	—0.071	—0.017	—0,144
a_2, Mbar	0.052	—0.069	0.737
a_3, Mbar	—0.693	—0.411	—1.8
a_4, Mbar	0.712	0.497	1.207

at T = 0 and P = 0). The dependence $\Theta(\rho)$ in Eq. (10) follows the Dugdale—MacDonald treatment. The parameters of the elastic interaction curve—P_C, are given in Table III.

Equation of state (10) is a quasiharmonic approximation and does not allow for the influence of the anharmonicity on the specific heat. It is applicable to the solid phase of NaCl and the first solid phase of KCl (KCl I). From the work of Bridgman[24] and Clark[14] it is known that KCl undergoes a phase transition at a pressure of about 19 kbar and temperatures from 300 to 1315° K, with practically no change in the entropy. This phase transition is observed also under dynamic conditions.[6] To describe this transition, we shall assume the free energy of the second KCl phase (KCl II) in the form

$$F_{II} = E_{cII} + 6RT\ln\frac{\Theta_{II}(\rho)}{T} + 6R(T_1 + c_1T). \quad (11)$$

The parameters of the last term in Eq. (11), which gives the difference between the energies of the two phases, are T_1 = 167° K, c_1 = −0.005. The assumed form of the dependence of this term is unimportant since it represents only a small correction.

The dynamic adiabats of NaCl, KCl I, and KCl II, calculated from the equations of state (10) and (11), are given in Figs. 7-9. Comparison with the experimental data plotted in the coordinates T—P and P—ρ shows that these equations of state describe satisfactorily the behavior of the solids right up to the melting curve.

An important result which follows from this comparison is that the influence of the anharmonicity on the specific heat of a solid ionic crystal is relatively small. The experimental data indicate rather that the specific heat of the lattice is somewhat higher than the Dulong—Petit value. Therefore, allowance for the influence of the anharmonicity in the solid-phase region of NaCl and KCl, made in [6,7], is unjustified because it reduces the specific heat. This can be seen clearly in Figs. 7 and 8. The difference between the calculated[6] and experimental values of temperatures for KCl (or at least half of this difference) is due to an inaccurate allowance for the conditions of phase equilibrium between the two solid phases of KCl.[6] For NaCl, the reduction in the specific heat is slight, both according to [7] and according to [6], so that the dependence T(P) given in [6] is in satisfactory agreement with experiment (this dependence fits the continuous curve in Fig. 7).

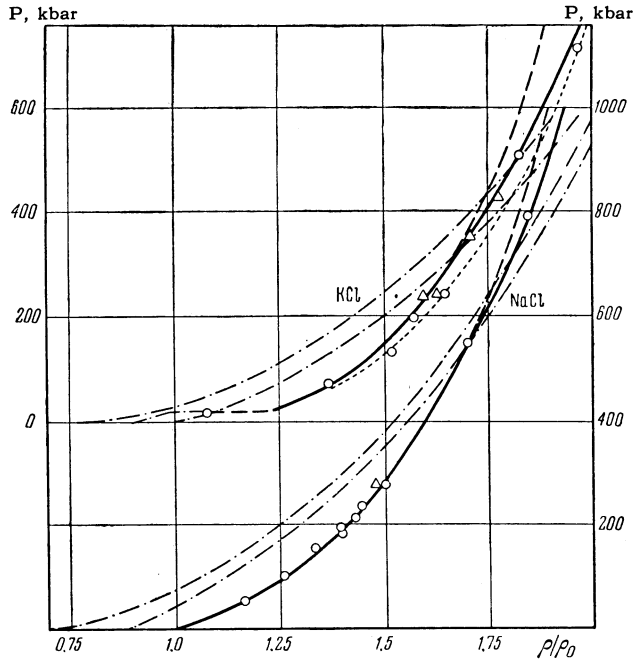

FIG. 9. Dynamic adiabats and regions of coexistence for NaCl and KCl: o – according to[4, 6], Δ – according to[7] and the present study. Continuous and dashed curves are, respectively, the calculated equilibrium and "superheated" shock adiabats; dotted curve is plotted in accordance with[6]; chain curves represent the boundaries of the regions of coexistence.

Knowing the equation of state for the solid phase and the experimental values of pressure, temperature, and density at the point where the shock adiabats leave the region of phase coexistence and enter the liquid-phase region, we can calculate the latent heat of fusion at the pressure corresponding to this point:

$$L = T_4\Delta S = E_0 + 0.5P_4(V_0 + V_4 - 2V_3) - E_3, \quad (12)$$

where E_0 and V_0 are, respectively, the internal energy and the volume of the substance ahead of the shock-wave front; P_4, V_4, and T_4 are, respectively, the pressure, volume, and temperature of the liquid phase behind the shock-wave front; E_3 and V_3 are, respectively, the internal energy and the solid phase volume at the pressure P_4 and temperature T_4 (the subscripts "3" and "4" follow the notation in Fig. 1). The experimental data necessary for the calculation of the latent

Table IV

	NaCl	KCl		NaCl	KCl
V_0, cm^3/g	0.4619	0.5015	E_3, kJ/g	6.32	4.51
E_0, kJ/g	0.174	0.147	L, kJ/g	1.39	1.50
P_4, kbar	700	480	ΔS, $J.g^{-1}deg^{-1}$	0.376	0.367
T_4, 10^3 °K	3.7	4.1	ΔS_0, $J.g.^{-1}.deg^{-1}$	0.452	0.335
V_4, cm^3/g	0.255	0.277	$\Delta V/V_3$, %	1.6	3.7
V_3, cm^3/g	0.251	0.267			

heat of fusion using Eq. (12) were taken from Figs. 7—9. From the dynamic adiabat of KCl (Fig. 9), we determined the parameters of three new points (cf. Table II), two of which were in the region of coexistence between the solid and liquid phases. This made it possible to improve somewhat the precision of the adiabat, compared with [6], in the region of greatest interest to us. All the initial data, together with the values of the entropy change when NaCl and KCl melt, are listed in Table IV.

The slopes of the melting curves, calculated from the Clapeyron—Clausius equation $dT/dp = \Delta V/\Delta S$ using the values of ΔV and ΔS found to be, respectively, 1.1×10^{-3} and 2.7×10^{-3} deg/bar. They were in good agreement with the experimental data (cf. double continuous lines in Figs. 7 and 8).

Several important conclusions may be drawn from the data in Table IV. From a comparison of the values of ΔS at low (P = 0 for NaCl and P = 19 kbar for KCl) and high pressures, it follows that the entropy change remains almost constant on the melting curves of the investigated crystals. At the same time, the change in volume decreases very markedly. Thus for NaCl at P = 0, the change in volume amounts to 20—25%, while at P = 700 kbar the change is $(V_4 - V_3)/V_3 \approx 2\%$. Similar behavior is observed also for KCl: the change in volume decreases from $\Delta V/V \approx 20\%$ at P = 19 kbar to $\approx 4\%$ at P = 480 kbar. Thus the experimental data obtained at these very high pressures indicate the absence of a critical point in the melting curves of NaCl and KCl. This conclusion confirms that drawn by Bridgman [25] from low-pressure data. The melting point, and, therefore, the latent heat of fusion (for ΔS = const) increase, under the conditions considered here, by a factor of 4 compared with the values at atmospheric pressure. This indicates that the height of the potential barrier which an ion has to overcome on leaving its lattice site, increases when the substance is compressed. It is interesting to note that the self-diffusion activation energy for metals increases proportionally to the melting point as pressure is increased. [26,27] Finally, from the fact that under pressure the change in the specific volume on melting becomes much smaller, it follows that under conditions of high compression the liquid state, at least at the melting point, differs much less in its properties from the solid state than at atmospheric pressure.

To describe the melting curve and the experimental data in the liquid-phase region, we shall write the free energy of the liquid phase in the form [4,17]

$$F_l = E_x + 6RT\ln\frac{\Theta(\rho)}{T} + 3RT\ln(1+z) - 6RT\left[b(\rho) - f(\rho)\frac{T_0}{T}\right], \qquad (13)$$

where

$$z = lRT\left(\frac{dP_c}{d\rho} - \frac{2P_c}{3\rho}\right)^{-1}, \quad f(\rho) = c + \frac{a}{r_1}\left[\left(\frac{\delta}{\delta_0}\right)^{r_1} - 1\right],$$

$$b = b_0 + \frac{b_1}{r_2}\left[\left(\frac{\delta}{\delta_0}\right)^{r_2} - 1\right],$$

and T_0 and δ_0 are, respectively, the temperature and relative density of the liquid phase at atmospheric pressure. The last term in Eq. (13) is introduced in [17] to describe the difference between the entropies and densities in the solid and liquid states. The unknown parameters in Eq. (13) are found from the properties of the substance at atmospheric pressure and from the experimental data given above. [5] For NaCl and KCl, these parameters are:

Parameter:	l	a	b_0	b_1	c	δ_0	r_1	r_2
NaCl:	12	1.505	0.5254	0	0.2358	0.7	0	—
KCl:	18	2.1	0.583	0.631	0.3108	0.747	—3	—3

Using the equations of state for the solid (10), (11) and the liquid (13) phases we calculated the dynamic adiabats and the melting curves of NaCl and KCl. The results of the calculations are shown in Figs. 7—9 and in Table V. Table V gives also the values (for the melting curve) of the change in the entropy and the parameter z, which

[5] For the liquid phase of KCl, we assumed the elastic curve of the first KCl phase, which was found with allowance for the experimental shock adiabat of the liquid phase.

Table V

Parameter	T/T_0 1.0	1.5	2.0	2.5	3.0	3.5	4.0
	NaCl, $T_0 = 1073°$ K						
P, kbar	0	29	83	167	324	607	1107
δ_T	0.8640	0.9342	1.0629	1.2174	1.4357	1.7159	2.0657
δ_J	0.7000	0.8383	0.9972	1.1674	1.3950	1.6813	2.0357
$\Delta S/6R$	0.6018	0.4222	0.3788	0.3667	0.3804	0.4009	0.4215
z	0.4528	0.3693	0.3061	0.2619	0.2128	0.1701	0.1350
	KCl, $T_0 = 1043°$ K						
P, kbar	0	37	77	138	225	347	516
δ_T	0.8736*	0.9775	1.0668	1.1796	1.31	1.4555	1.6167
δ_J**	0.7470	1.0106	1.1385	1.2782	1.435	1.6062	1.7971
$\Delta S/6R$	0.5100	0.4327	0.4326	0.4571	1.4868	0.5173	0.5453
z	0.5042	0.3133	0.3131	0.3018	0.2833	0.2632	0.2416

*Here $\rho_c = 2.046$ g/cm^3, but in other columns of the same row $\rho_c = 2.36$ g/cm^3.
**In this row $\rho_c = 2.046$ g/cm^3.

Table VI

	Present study				According to[14]			
	P_0, kbar	A, kbar	q	$T_0°$, K	P_0, kbar	A, kbar	q	$T_0°$, K
NaCl	0	15	3	1073	0	16.7	2.7	1073
KCl	18.95	16.1	3	1315	18.95	12.1	4	1315

reflects the difference between the specific heat and the Grüneisen parameter of a liquid and the same parameters of a solid.[7] From Figs. 7—9, it is evident that the experimental data are described satisfactorily by the assumed equations of state. The calculated melting curve of NaCl also describes the experimental data obtained in static measurements.[14] This is understandable because in choosing the parameters in the equation of state of the liquid phase it has been possible to use the initial value of the slope of the melting curve given in[14]. We were unable to match our experimental data for KCl with the melting curve in[14]. It is possible that this is due to the more complex dependence of the functions b and f on the density.

The melting curves, calculated from Lindemann's formula ($T_{melt} \sim dP_c/d\rho - 2P_c/3\rho$),[16,15] pass quite close to the experimental curves. The differences of 35% at P = 700 kbar for NaCl and 25% at 500 kbar for KCl should be regarded as small for such a simple model. However, contrary to the experimental data these calculated curves are characterized (cf. Figs. 7 and 8) by a small value of dT/dP at P = 0 and a large value at P ≈ 0.5—1 Mbar. To a lesser degree, this applies also to the melting curves in Simon's form. In Figs. 7 and 8, the melting curves, calculated from Eq. (1), are given in two variants: with Simon's coefficients found by Clark[14] and with coefficients selected (see the left-hand part of Table VI) to give the best fit with our experimental data. Simon's equations with these new coefficients also describe well the data in[14], since the initial slope of the melting curves is not greatly affected by this procedure.

We shall consider two other problems. It has been mentioned in[7] that at U ≥ 3.5 km/sec the D—U relationships of KCl and KBr exhibit a discontinuity. The present results indicate that, at least for KCl, this discontinuity represents the melting of the substance. No such discontinuity in the D—U relationship has been found when NaCl melts (cf. Fig. 10). This is possibly due to the reduction in the coordination number when KCl II melts, the solid phase of which has the CsCl structure, more closely packed than NaCl. Another problem is whether melting gives rise to a two-wave configuration (the breakup of a shock wave into two waves). It is known that phase transitions occurring behind the shock-wave front may produce this situation. As shown in[13,28,17], the appearance of the two-wave configuration depends on the slope of the melting curve. In our case, the experimental values of the melting curve slopes at the points where they intersect with the shock adiabats of the solid phases NaCl and KCl II are such that the two-wave configuration could not have arisen.

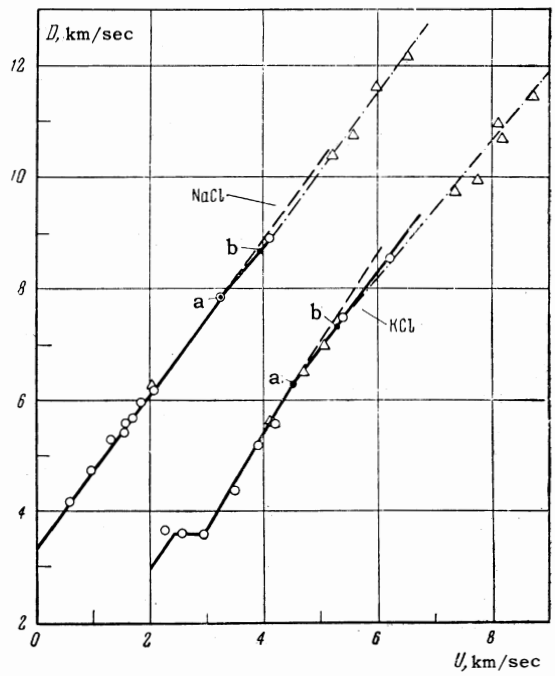

FIG. 10. D–U relationships for NaCl and KCl (values of U for KCl are increased by 2 km/sec): o – according to[4, 6], Δ – according to[7] and the present study; the continuous and dashed curves represent, respectively, the calculated equilibrium and "superheated" shock adiabats; the chain curve is taken from[7]; a) beginning of melting; b) end of melting.

In the limiting case, the two-wave configuration may appear when the wave ray 0–2 (Fig. 1b) is a tangent to the region of coexistence with the liquid phase (curve 2–3, Fig. 1b): $dP/dV = P_2/(V_2 - V_0)$. The slopes of a melting curve in the coordinates T–P and P–V are related by

$$\frac{dT}{dP} = \left[1 - \left(\frac{\partial P}{\partial V}\right)_T \Big/ \frac{dP}{dV}\right] \Big/ \left(\frac{\partial P}{\partial T}\right)_V, \qquad (14)$$

where the partial derivatives are found from the equation of state for the solid phase (10), (11). For example, for KCl at $P_2 = 330$ kbar, $V_2 = 0.2963$ cm^3 and $T_2 = 3800°$ K we have

$$\left(\frac{\partial P}{\partial T}\right)_V = 3{,}37 \text{ J} \cdot \text{cm}^{-3} \cdot \text{deg}, \quad \left(\frac{\partial P}{\partial V}\right)_T = 380 \text{ kJ} \cdot \text{g} \cdot \text{cm}^{-6}$$

$$\frac{dP}{dV} = \frac{P_2}{V_2 - V_0} = -161 \text{ kJ} \cdot \text{g} \cdot \text{cm}^{-6}$$

and from Eq. (14) we obtain $dT/dP < -0.4$ deg/bar. This value clearly contradicts the experimental slope of the melting curve, obtained in the present work (cf. Fig. 8). A similar result is obtained for NaCl.

The absence of the two-wave configuration in KCl is confirmed also by the measurements of the wave velocities at various shock-wave intensities in the region of the coexistence of phases. It is evident from Fig. 10 that the characteristic "step" in the D–U relationship is absent.

[1] Walsh, Rice, McQueen, and Yarger, Phys. Rev. **108**, 196 (1957).
[2] Al'tshuler, Krupnikov, Ledenev, Zhuchikhin, and Brazhnik, JETP **34**, 874 (1958), Soviet Phys. JETP **7**, 606 (1958).
[3] Al'tshuler, Kormer, Bakanova, and Trunin, JETP **38**, 790 (1960), Soviet Phys. JETP **11**, 573 (1960).
[4] Al'tshuler, Kuleshova, and Pavlovskiĭ, JETP **39**, 16 (1960), Soviet Phys. JETP **12**, 10 (1961).
[5] Kormer, Funtikov, Urlin, and Kolesnikova, JETP **42**, 686 (1962), Soviet Phys. JETP **15**, 477 (1962).
[6] Al'tshuler, Pavlovskiĭ, Kuleshova, and Simakov, FTT **5**, 279 (1963), Soviet Phys. Solid State **5**, 203 (1963).
[7] Kormer, Sinitsyn, Funtikov, Urlin, and Blinov, JETP **47**, 1202 (1964), Soviet Phys. JETP **20**, 811 (1965).
[8] Zel'dovich, Kormer, Sinitsyn, and Kuryapin, DAN SSSR **122**, 48 (1958), Soviet Phys. Doklady **3**, 938 (1959).
[9] Ya. B. Zel'dovich and Yu. P. Raĭzer, JETP **35**, 1402 (1958), Soviet Phys. JETP **8**, 980 (1959).
[10] J. Taylor, J. Appl. Phys. **34**, 2727 (1963).
[11] I. Sh. Model', JETP **32**, 714 (1957), Soviet Phys. JETP **5**, 589 (1957).
[12] Zel'dovich, Kormer, Sinitsyn, and Yushko, DAN SSSR **138**, 1333 (1961), Soviet Phys. Doklady **6**, 494 (1961).
[13] V. D. Urlin and A. A. Ivanov, DAN SSSR **149**, 1303 (1963), Soviet Phys. Doklady **8**, 380 (1963).
[14] S. P. Clark, Jr., J. Chem. Phys. **31**, 1526 (1959).
[15] J. J. Gilvarry, Phys. Rev. **102**, 308 (1956).
[16] F. A. Lindemann, Phys. Z. **11**, 609 (1910).
[17] V. D. Urlin, JETP (in press).
[18] G. Ribo, Opticheskaya pirometriya (Optical Pyrometry) GTTI, 1934.
[19] Vil'dgrube, Dunaevskaya, and Kharitonova, PTÉ No. 6, 91 (1961).
[20] Voĭtenko, Kuznetsov, and Model', PTÉ No. 6, 121 (1962).
[21] Grenishin, Solodovnikov, and Startsev, Tr. Komissii po pirometrii pri VNIIM (Proceedings of the Commission on Pyrometry of the D. I. Mendeleev All-Union Metrology Research Institute), No. 1, Standartgiz, 1958.
[22] Pavlovskiĭ, Vashchenko, and Simakov, FTT **7**, 1212 (1965), Soviet Phys. Solid State (in press).

[23] Al'tshuler, Kormer, Brazhnik, Vladimirov, Speranskaya, and Funtikov, JETP **38**, 1061 (1960), Soviet Phys. JETP **11**, 766 (1960).
[24] P. W. Bridgman, Phys. Rev. **57**, 237 (1940).
[25] P. W. Bridgman, The Physics of High Pressure, Bell, London, 1931.
[26] Nachtrieb, Weil, Catalano, and Lawson, J. Chem. Phys. **20**, 1189 (1952).
[27] Nachtrieb, Resing, and Rice, J. Chem. Phys. **31**, 135 (1959).
[28] N. M. Kuznetsov, DAN SSSR **155**, 156 (1964).

Translated by A. Tybulewicz
150